

# Extraordinary Optical Transmission through Single Sub-Wavelength Slot Nano Antennas

Mohamed S. Fouad<sup>1,2</sup>, Mohamed Nady<sup>3</sup>, AbdelHamid AbdelMonem Shaalan<sup>2</sup>

<sup>1</sup>High Institute of Electronic Engineering (EEI), Ministry of Higher Education, Belbes, Elsharkia, Egypt

<sup>2</sup>Department of communication and electronics, Faculty of Engineering, Zagazig University, Elsharkia, Egypt

<sup>3</sup>Microwave Engineering Department, Electronics Research Institute (ERI), Cairo, Egypt

Email: mohameds.fouad4@gmail.com, dr.mnady2014@gmail.com, ashaalan@zu.edu.eg, shaalan\_zag2010@yahoo.com

**How to cite this paper:** Fouad, M.S., Nady, M. and Shaalan, A.A. (2019) Extraordinary Optical Transmission through Single Sub-Wavelength Slot Nano Antennas. *Optics and Photonics Journal*, 9, 112-125.  
<https://doi.org/10.4236/opj.2019.97011>

**Received:** May 30, 2019

**Accepted:** July 26, 2019

**Published:** July 29, 2019

Copyright © 2019 by author(s) and Scientific Research Publishing Inc.

This work is licensed under the Creative Commons Attribution International License (CC BY 4.0).

<http://creativecommons.org/licenses/by/4.0/>



Open Access

## Abstract

This paper investigates the electromagnetic transmission through the sub-wavelength slot model on a metal film for TM- and TE-polarized light. The influence of several parameters such as the slot width, the metal film thickness and the polarization of the incident field is investigated using FDTD method. The FDTD simulation's results have shown that the sub-wavelength slot in the metal films has extraordinary optical transmission (EOT) properties for TM-polarized light. The EOT has been observed as being symmetrically punctured and characterized by the appearance of a series of transmission peaks and dips in the transmission field. By varying the slot thickness we have investigated the effect of the Fabry-Pérot like resonance in the sub wavelength slot. This component can be a key element in many applications. High-spatial-resolution imaging and information and communications technologies and sensing with high spectral and spatial precision, enhanced solar cells, efficient optical sources and detectors, disease treatment, are such examples.

## Keywords

Slot Nano-Antennas, Plasmonics Waveguides

## 1. Introduction

Unluckily, the fundamental laws of diffraction limit the size of photonics, while the interconnect RC delay-time issues limit the speed of semiconductor electronics. Over the last two decades, it has gradually become clear that the plasmonic devices can play in the future technologies to complement conventional photonics and electronics. Plasmonics offers exactly what electronics and pho-

tonics do not have, *i.e.* the size of electronics and the speed of photonics [1]. In addition, plasmonic devices might logically interface with comparative-speed photonic devices and with comparative-size electronic components, so, expanding the collaboration between these technologies. Therefore it can serve as a bridge between similar-size nano-electronics and similar-speed dielectric photonics.

Plasmonics technologies have grown rapidly over the last two decades due to the exciting physical properties of Surface Plasmon Polaritons (SPPs). SPPs are quantized charge density oscillations occurring at the interface between the free electron gas of a metal and a dielectric material. The nature of these quasi-particles is that of an electromagnetic wave trapped at the surface between such two media. Motions of the charge density drive the electromagnetic wave, which can propagate for relatively large distances across the surface of the interface (in the order of micrometers, or even millimeters relying upon the materials and the frequency of operation). Even though surface-enhanced Raman spectroscopy (SERS), being the first applications of surface Plasmon metallic nanostructures, was discovered in the 1970s [2] [3], the field of plasmonics started to rapidly spread in the early 2000s. Around then it was exhibited that metallic nanowires can guide light well below the diffraction limit [4]; a simple thin film of metal can serve as an optical lens [5]; and sliver films with nano-scale holes show extraordinarily optical transmission (EOT) [6]. The most essential applications in the plasmonics field appear to depend on one key property of engineered metallic structures that is the ability to guide and concentrate light at the nano-scale [7] [8] [9] [10] [11]. It is envisaged that plasmonics, combined with nano photonics, has the potential to provide ultra-small optoelectronic components having higher speeds and greater bandwidths. Investigations involve building, manipulating, and characterizing optically active nanostructures to innovate new capabilities for the nano-scale high-spatial-resolution imaging [12] [13] [14] and information and communications technologies [15] and sensing with high spectral and spatial precision [16] [17], coupling devices [18], enhanced solar cells [19] [20] [21], efficient optical sources [22] [23] [24] and ultrafast acousto-magneto-plasmonics [25] detectors [26], disease treatment [27] [28], nano laser [29], and many other applications. In spite of the fact that the basics for SPPs are well established, SPPs based structures are complex. Therefore, it is frequently not possible to achieve analytical solutions that characterize the operation of a device; in this way the numerical modeling becomes an essential tool to analyze and investigate the operation of such structures. Numerous numerical techniques have been developed, such as Finite Element Method (FEM) [30], Finite-Difference Time-Domain (FDTD) [31], Beam propagation method (BPM) [32], Method of Moment (MOM) [33] etc. Due to the known limitations in accuracy achievable using BPM and MOM [32] [33], when modeling discrete structures such as slots with sharp structural transitions, it is not used heavily. In this paper, the numerical models have been primarily based on FDTD. In this paper, the light transmission through a single sub-wavelength slot is discussed.

The influence of several parameters such as the slot width, the metal film thickness and the polarization of the incident field are investigated using FDTD method. The simulation results show that a sub-wavelength slot in the gold metal films has extraordinary optical transmission properties (EOT). The EOT is observed as being symmetrically perforated and characterized by the appearance of a series of transmission peaks and dips in the transmission spectrum. This paper is organized as follows: Section 2 introduces the proposed model and its dimension and materials parameters; Section 3 describes the FDTD method where the parameters needed to simulate this model is presented. The results are presented in Section 4. Finally, Section 5 summarizes our concluded remark.

## 2. The Single Sub-Wavelength Slot Model

In the next sections we will study the conditions of propagation inside an infinitely long metallic slot. A schematic of the system is represented in **Figure 1(a)** thin dielectric layer (air)  $\epsilon_r = 1$  of width  $w$  and thickness  $t$  and depth  $L$  permittivity  $\epsilon_d = 1$  is sandwiched between two semi-infinite metal areas (gold Au) of permittivity  $\epsilon_m$ . (Au) is the second most significant metal after silver for plasmonic applications [34]. It is widely chosen for many applications over silver because of its stability. Moreover, Au is an easily accessible material that can be evaporated to a thin smooth layer on a surface. Because of these two reasons, throughout this paper, we will concentrate our focus on gold. Au dispersive permittivity can be denoted by the Drude model [35].

$$\epsilon(\omega) = \epsilon_\infty - \omega_p^2 / (\omega^2 + i\omega\gamma) \quad (1)$$

where  $\omega$  is the angular frequency of the incident light,  $\epsilon_\infty$  the dielectric constant at an infinite angular frequency and equals 3.7,  $\omega_p$  the bulk plasma frequency and equals  $1.3709 \times 10^{16}$  rad/s, and  $\gamma$  the electron collision frequency equals  $4.059 \times 10^{13}$  rad/s [36]. A simplified picture of the 2D slot in a metal layer **Figure 1** is that of a waveguide, where the nano-slot forms a vertical metal insulator-metal (MIM), [37] [38] [39] waveguide of finite length with thickness  $t$ . The 2D Finite Difference Time Domain (FDTD) method allows us to directly use experimental data for the frequency-dependent dielectric constant of metals such as gold including both the real and imaginary parts, with no further approximation.

## 3. FDTD Model

In this section, we investigate the nano slot properties of the nano slot waveguide in a two dimensional (2D) plasmonic waveguide with Au-air-Au interfaces using a finite-difference-time-domain (FDTD) method [40] and perfectly matched-layer (PML) as an absorbing boundary condition (ABC). In our numerical calculations with FDTD, the nano slot waveguide are described by a spatial discretization mesh. A spatial mesh size of  $\Delta x = \Delta y = 9$  nm in the FDTD algorithm is found sufficient for convergence of the numerical results. Calculations in FDTD are performed according to the steps listed in **Figure 2** [41] [42].

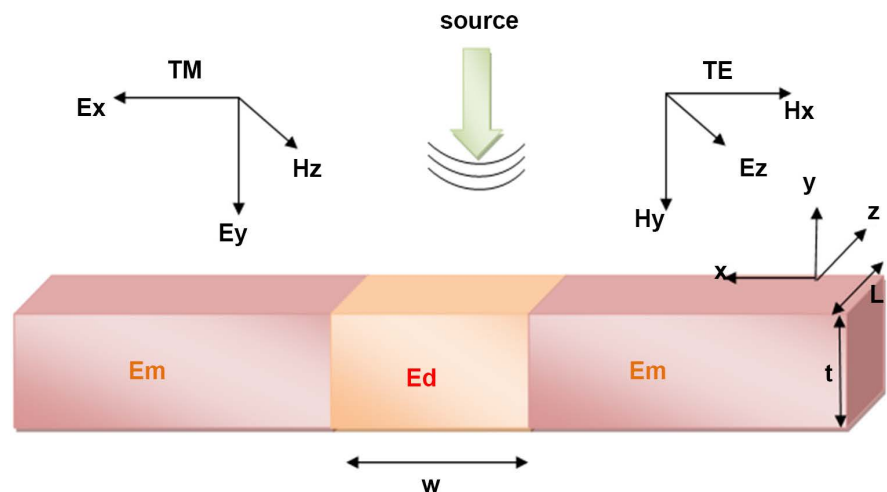


**Figure 1.** Schematic of the single sub-wavelength slot structure and parameters' definitions used for the structure dimensions and incident light field directions.

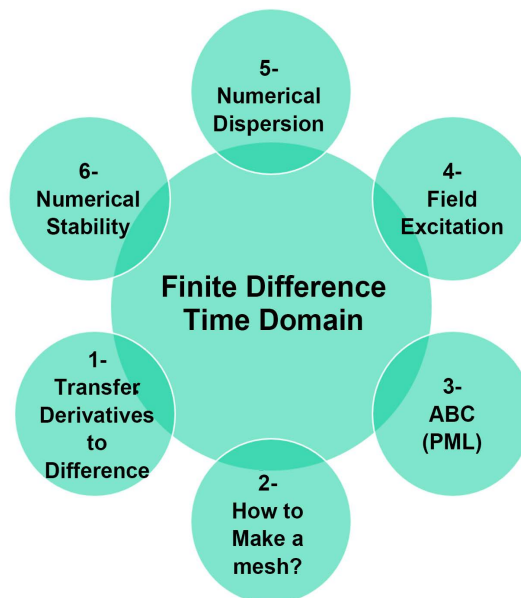


**Figure 2.** Layout of FDTD method [42].

This system is made up of a 2D box (along the  $x$  &  $y$ -axes) with propagation along the  $y$ -axis. UPML boundary conditions are applied at both boundaries in  $y$  and  $x$  of the box in order to eliminate the reflection of outgoing waves [41]. 50 nm width for the PML is found to be thick enough to fully absorb outgoing waves. The structure is supposed to be infinite along the  $z$ -direction. The equations of motion are solved with a time integration step  $\Delta t = (\Delta x/4c) = 20.88 \times 10^{-18}$  seconds to avoid the problems of numerical dispersion and stability. The number of time steps is equal to 2, which is the necessary tested time for good convergence of the numerical calculations.

The wavelength of the incident light,  $\lambda_0 = 830$  nm, which lies in the near-infrared range.

## 4. Numerical Results

After the presentation of our analysis for the propagation characteristics of the electromagnetic waves through the nano slots. The structure presented in **Figure 1** is studied in two different cases; the TE and TM. Where, the direction of propagation is the y direction and the wavelength of the incident light equals  $\lambda_0 = 830$  nm.

### 4.1. TE-Polarization

The structure displayed in **Figure 1** is simulated using FDTD technique under the TE polarized incident wave. **Figure 2** shows the simulated EM field distributions ( $H_x$ ,  $H_y$  and  $E_z$ ) for a sub-wavelength slot with  $W = 350$  nm (*i.e.*,  $< 1/2\lambda_0$ ) and 300 nm film thickness. The weak EM fields down to the hole demonstrate that no light transmits through the sub-wavelength slot.

The electric field at the top metal surface is approximately zero (see the  $|E_z|$  field distribution in **Figure 3**), while  $H_x$  at this region is a maximum. This is due to the fact that because Maxwell's equations require  $E_z$  to be continuous at the interface, and negligible inside the metal. As seen in **Figure 2**, very little electric field is needed to oscillate the surface conduction electrons, and thus to establish the  $J_z$  surface current. In contrast, continuity at the interface is not required for  $H_x$  because of the existence of the surface current  $J_z$  [43].

As seen in **Figure 3**, the incident electric and magnetic fields carry the EM energy in through the sub-wavelength aperture, while the metallic film sends a strong reflected beam back. For a metal film with no aperture, these counter-propagating beams form a standing wave above the upper surface. The penetrating  $E_z$  creates a surface current  $J_z$  along the slot walls, which, in turn produce an  $H_y$  on the walls' exterior surfaces as seen in  $|H_y|$  field distribution.

When  $W < 0.5 \lambda_0$ , very little light transmits through the sub-wavelength slot and the incident EM wave is reflected back. These simulations for TE-polarized incident light revealed the existence of a cut-off at around  $W \approx 0.5\lambda_0$  for TE-polarized waves through the sub-wavelength slot. In contrast, as shown in **Figure 4**, when  $W = 500$  nm (*i.e.*,  $> 1/2\lambda_0$ ), there is little attenuation and the EM waves transmit through the slot.

In **Figure 5**, we show the simulated field distribution of the pointing vector  $p_y$  (*i.e.*, energy flowing along the y direction) under TE-polarized incident light for two values of the sub wavelength slot width;  $W = 350$  nm (*i.e.*, below cut-off) and  $W = 500$  nm. Decreasing the slot-width below the slot cut-off reduces the transmission as shown in **Figure 5(a)** [43] [44].

### 4.2. TM-Polarization

The simulations described in this section show the demonstration of a cut-off for TM-polarized incident light with extraordinary light transmission, even for an aperture as narrow as  $W = 0.01\lambda_0$ . Transmission is seen to be the result of strong electric and magnetic fields that propagate along the sub-wavelength slot walls,

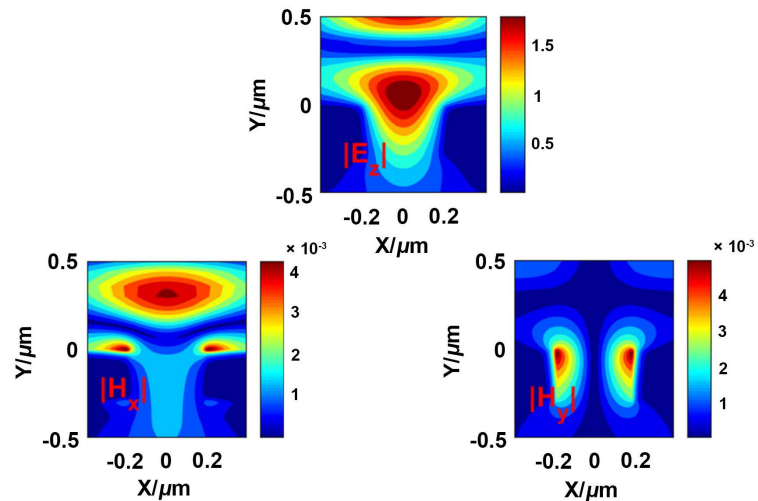


**Figure 3.** Simulated field distribution of  $|E_z|$ ,  $|H_x|$  and  $|H_y|$  with TE-polarized incident light for film thickness  $t = 300$  nm and slot width  $W = 350$  nm.

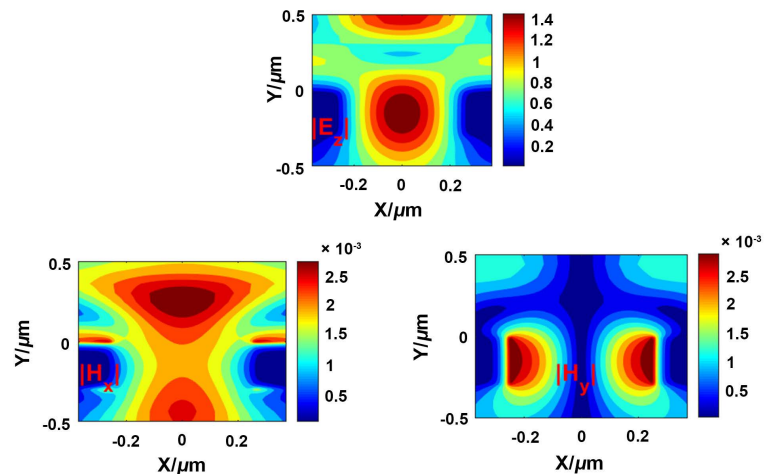


**Figure 4.** Simulated field distribution of  $|H_x|$ ,  $|H_y|$  and  $|E_z|$  with TE-polarization incident light for film thickness  $t = 300$  nm and slot width  $W = 500$  nm.

being supported by the appropriate distribution of surface charges on these walls. **Figure 6** shows simulated field allocation of  $|E_x|$ ,  $|E_y|$  and  $|H_z|$  for a 100 nm slot width in a 300 nm Au film thickness.

As for TE illumination, very little  $E_x$  is needed on the top metal surface to sustain the  $J_x$  surface current which supports the magnetic field  $H_z$  immediately above the surface. The reflected  $E_x$  and  $H_z$  interfere with the incident fields to produce standing waves above the top surface. The surface current stops at the edges of the slot, giving rise to accumulated charges at the slot corners (see  $|E_y|$  field distribution in **Figure 6**). These oscillating charges, on opposite edges of the slot, act as an electric dipole. These surface charges play a role in enhancing transmission through the slot [45]. Inside the slot, the surface charges and currents carry the travelling beam along the slot; it creates a second electric dipole as seen in the  $E_y$  distribution field displayed in **Figure 6**.

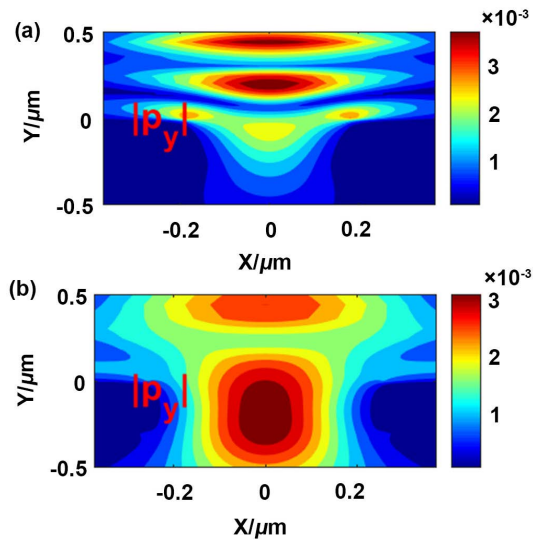


**Figure 5.** Simulated field distribution of  $|p_y|$  with TE-polarized incident light for a film thickness  $t = 300$  nm and slot width (a)  $W = 350$  nm and (b)  $W = 500$  nm.

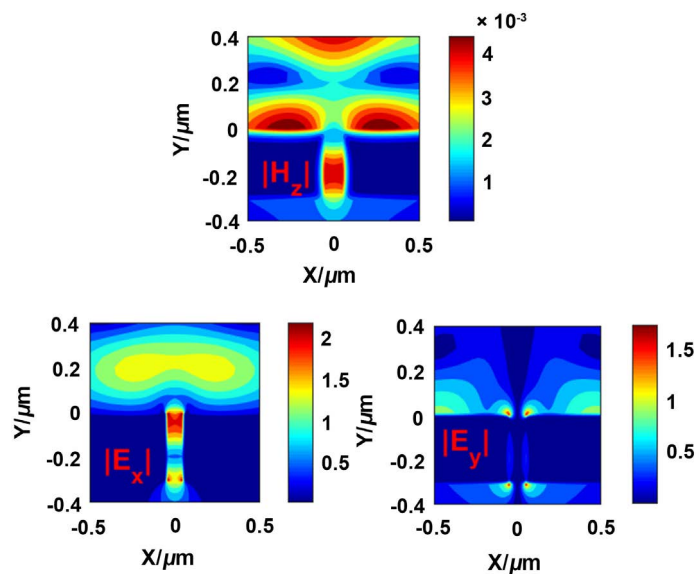


**Figure 6.** Simulation field distribution of  $|H_z|$ ,  $|E_x|$  and  $|E_y|$  for a film thickness of  $t = 300$  nm and aperture width of  $W = 100$  nm with TM-polarized incident light.

For the sub-wavelength slot with thickness of  $t = 500$  nm, only one strong dipole is observed at the bottom of the slot (see  $|E_y|$  distribution field in **Figure 7**).

The charges that produce the dipole at the top of the slot have diminished, and the transmission efficiency is substantially reduced compared with the 300 nm film thickness. It appears that the distractive interference between two counter-propagating beams within the slot is responsible for the reduced transmission efficiency in this case [43]. The metal film thickness of  $t = 300$  nm and 500 nm are not the only interesting cases with large transmission. At  $t = 600$

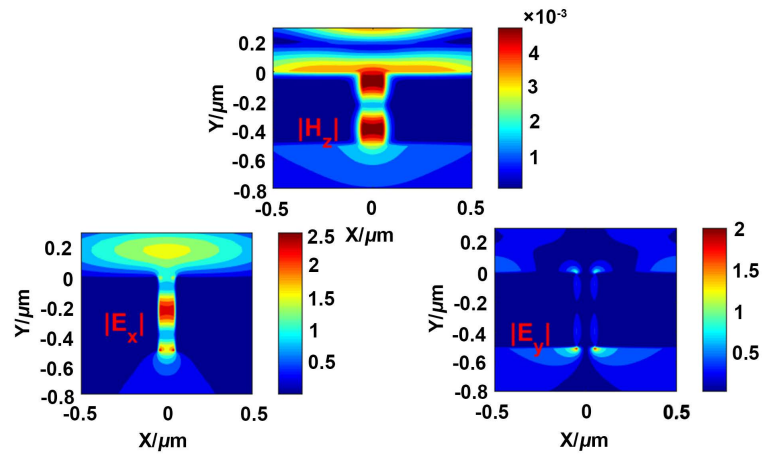


**Figure 7.** Simulated field distribution of  $|H_z|$ ,  $|E_x|$  and  $|E_y|$  for a film thickness of  $t = 500$  nm and aperture width of  $W = 100$  nm with TM-polarized incident light.

nm strong electric dipoles once again at the sharp edges of the slot (see  $|E_y|$  and  $|E_x|$  fields allocation in **Figure 8**), and the great transmission is subsequently observed. The difference with the case of  $t = 600$  nm is that, in the middle of the metal film the charges disappear while the wall surface current in that region reaches a maximum (see the  $|H_z|$  field distribution in **Figure 8**). It is evident that a strong current along the slit walls creates the top and bottom dipoles.

As shown in the  $|E_x|$  and  $|E_y|$  fields distribution in (**Figure 8**). The charges are accumulated in three places on each side of the slot walls: in the middle of the film and at the top and bottom corners of the slot. Also, the current on the slot walls is apparently stronger than that on the top surface as seen in the  $|H_z|$  field distribution in **Figure 8**.

In **Figure 9** we show the simulated field distribution of the simulated pointing vector  $p_y$  (*i.e.*, energy flowing along the  $-y$  direction) under TM-polarized incident light for the three values of the metal film thickness;  $t = 300$  nm, 500 nm and 600 nm for 100 nm sub-wavelength slot width.

In **Figure 10** we summarize the study of the energy flux (*i.e.*, power) transmitted for an 830 nm TM-polarized incident light for different sub-wavelength slot thicknesses. The results are shown for a 100 nm wide slot while the Au film thickness varies from 50 nm to 600 nm with 20 nm increments.

The normalized transmitted power throughput from the sub-wavelength slot oscillates periodically as the Au thickness increases shows series of Fabry-Pérot like resonance. The transmission is maximal due to constructive interference when thickness  $t$  gives a length phase of even integer of  $\pi/2$  and is minimal when thickness  $t$  corresponds to a length phase of odd integer of  $\pi/2$ . As seen from **Figure 10**, the maximum normalized transmission power is always greater than the unity (*i.e.* extraordinary transmission). These results indicate that some of the incident photons outside of the sub-wavelength slot area are either captured and “funneled” through the slot to the transmission region or the transmission is

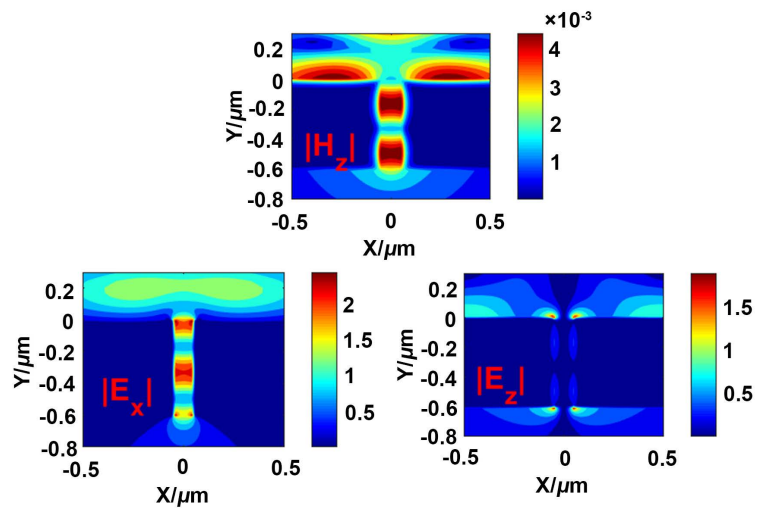


**Figure 8.** Simulated field distribution of  $|H_z|$ ,  $|E_x|$  and  $|E_y|$  for a film thickness of  $t = 600$  nm and aperture width of  $W = 100$  nm with TM-polarized incident light.

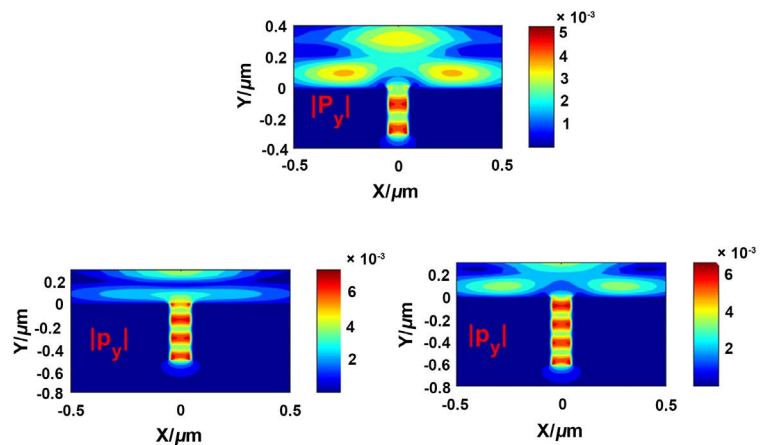


**Figure 9.** Simulated field distribution of  $|p_y|$  with TM-polarized incident light for a slot width  $W = 100$  nm and film thickness of (a)  $t = 300$  nm, (b)  $t = 500$  nm, (c)  $t = 600$  nm.

enhanced through the SPP waves which contribute to the final transmission power.

In **Figure 11** we summarize the study of the energy flux (*i.e.* power) transmitted for wavelengths from a 500 nm to 1500 nm TM-polarized incident light. The results are shown for different slot widths; 300, 400, and 500 nm. It is well known from the electromagnetics theory that the cut-off frequency of the waveguide depends mainly on the width of the waveguide. It is clear from this figure that for each structure there is a resonance wavelength. This resonance wavelength increases as the width of the slot increases. In other words, as the width of the slot is reduced the cut off frequency increases while the cut off wavelength is decreased. In these interpretations, we considered the slot as a waveguide. Each waveguide has a dominant cutoff wavelength. For example at width equals 300 nm

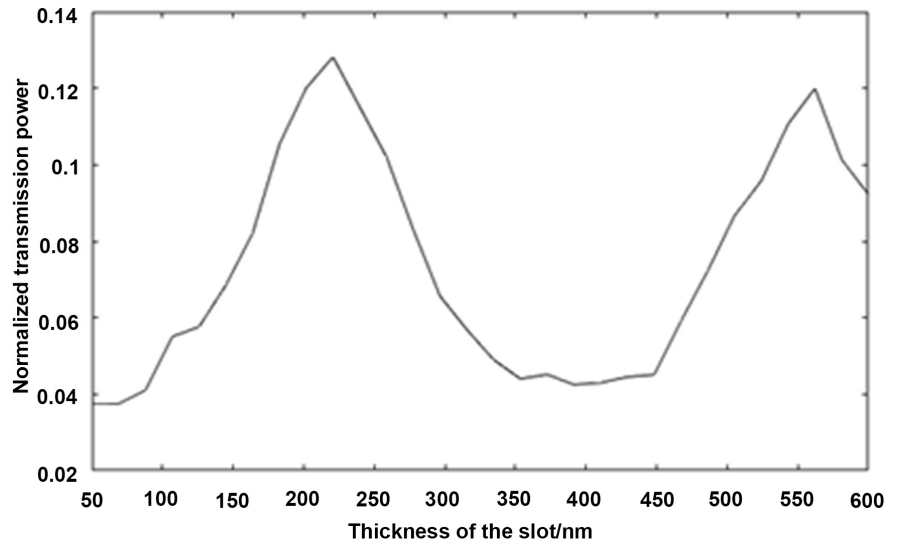


**Figure 10.** Normalized transmission power versus sub-wavelength slit thickness with 100 nm width.

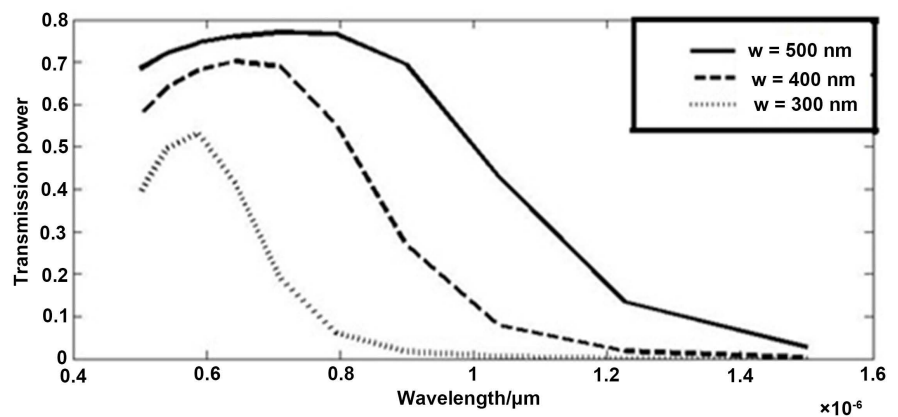


**Figure 11.** Normalized transmission power versus sub-wavelength for different widths.

waves at wavelength 800 nm will not transmit, while it will transmit for width 500 nm.

## 5. Conclusion

The transmission through the sub-wavelength slot model on a metal film, namely gold, for TM- and TE-polarized light has been investigated in this paper. The FDTD simulation's results have shown that the sub-wavelength slot in the metal films has extraordinary optical transmission (EOT) properties for TM-polarized light. The effect of different parameters has been studied such as width, thickness, and polarization of the incident wave. In these interpretations, we considered the slot as a waveguide. Each waveguide has a dominant cutoff wavelength. The EOT has been observed as being symmetrically perforated and characterized by the appearance of a series of transmission peaks and dips in the transmission field. By varying the slot thickness we have investigated the effect

of the Fabry-Pérot like resonance in the sub wavelength slot. This component can be a key element in many applications such as high-spatial-resolution imaging and information and communications technologies and sensing with high spectral and spatial precision, enhanced solar cells, efficient optical sources and detectors, disease treatment which are such examples.

### Conflicts of Interest

The authors declare no conflicts of interest regarding the publication of this paper.

### References

- [1] Raether, H. (1988) Surface Plasmons on Smooth Surfaces. In: *Surface Plasmons on Smooth and Rough Surfaces and on Gratings* (pp. 4-39). Springer, Berlin, Heidelberg.
- [2] Jeanmaire, D.L. and Van Duyne, R.P. (1977) Surface Raman Spectroelectrochemistry: Part I. Heterocyclic, Aromatic, and Aliphatic Amines Adsorbed on the Anodized Silver Electrode. *Journal of Electroanalytical Chemistry and Interfacial Electrochemistry*, **84**, 1-20. [https://doi.org/10.1016/0368-1874\(77\)80399-7](https://doi.org/10.1016/0368-1874(77)80399-7)
- [3] Fleischmann, M., Hendra, P.J. and McQuillan, A.J. (1974) Raman Spectra of Pyridine Adsorbed at a Silver Electrode. *Chemical Physics Letters*, **26**, 163-166. [https://doi.org/10.1016/0009-2614\(74\)85388-1](https://doi.org/10.1016/0009-2614(74)85388-1)
- [4] Takahara, J., Yamagishi, S., Taki, H., Morimoto, A. and Kobayashi, T. (1997) Guiding of a One-Dimensional Optical Beam with Nanometer Diameter. *Optics Letters*, **22**, 475-477. <https://doi.org/10.1364/OL.22.000475>
- [5] Pendry, J.B. (2000) Negative Refraction Makes a Perfect Lens. *Physical Review Letters*, **85**, 3966. <https://doi.org/10.1103/PhysRevLett.85.3966>
- [6] Ebbesen, T.W., Lezec, H.J., Ghaemi, H.F., Thio, T. and Wolff, P.A. (1998) Extraordinary Optical Transmission through Sub-Wavelength Hole Arrays. *Nature*, **391**, 667. <https://doi.org/10.1038/35570>
- [7] Barnes, W.L., Dereux, A. and Ebbesen, T.W. (2003) Surface Plasmon Subwavelength Optics. *Nature*, **424**, 824. <https://doi.org/10.1038/nature01937>
- [8] Schuller, J.A., Barnard, E.S., Cai, W., Jun, Y.C., White, J.S. and Brongersma, M.L. (2010) Plasmonics for Extreme Light Concentration and Manipulation. *Nature Materials*, **9**, 193. <https://doi.org/10.1038/nmat2630>
- [9] Brongersma, M.L. and Shalaev, V.M. (2010) The Case for Plasmonics. *Science*, **328**, 440-441. <https://doi.org/10.1126/science.1186905>
- [10] Stockman, M.I. (2011) Nanoplasmonics: The Physics behind the Applications. *Physics Today*, **64**, 39-44. <https://doi.org/10.1063/1.3554315>
- [11] Krajnik, B., Czechowski, N., Piatkowski, D., Mackowski, S., Hofmann, E., Pichler, S. and Heiss, W. (2013) Influence of Plasmon Excitations in Au Nanoparticles upon Fluorescence and Photostability of Photosynthetic Complexes. *Optics and Photonics Journal*, **3**, 1. <https://doi.org/10.4236/opj.2013.31001>
- [12] Vander, R. and Lipson, S.G. (2009) High-Resolution Surface-Plasmon Resonance Real-Time Imaging. *Optics Letters*, **34**, 37-39. <https://doi.org/10.1364/OL.34.000037>
- [13] Yao, J., Stewart, M.E., Maria, J., Lee, T.W., Gray, S.K., Rogers, J.A. and Nuzzo, R.G. (2008) Seeing Molecules by Eye: Surface Plasmon Resonance Imaging at Visible Wavelengths with High Spatial Resolution and Submonolayer Sensitivity. *Angewandte Chemie International Edition*, **47**, 1011-1014. <https://doi.org/10.1002/anie.200703001>

- wandte *Chemie International Edition*, **47**, 5013-5017.  
<https://doi.org/10.1002/anie.200800501>
- [14] Shan, X., Diez-Pérez, I., Wang, L., Wiktor, P., Gu, Y., Zhang, L. and Li, J. (2012) Imaging the Electrocatalytic Activity of Single Nanoparticles. *Nature Nanotechnology*, **7**, 668. <https://doi.org/10.1038/nnano.2012.134>
- [15] Jung, K.Y., Teixeira, F.L. and Reano, R.M. (2007) Au/SiO<sub>2</sub> Nanoring Plasmon Waveguides at Optical Communication Band. *Journal of Light Wave Technology*, **25**, 2757-2765. <https://doi.org/10.1109/JLT.2007.902100>
- [16] Kashyap, R. and Nemova, G. (2009) Surface Plasmon Resonance-Based Fiber and Planar Waveguide Sensors. *Journal of Sensors*, **2009**, Article ID: 645162. <https://doi.org/10.1155/2009/645162>
- [17] Pala, R.A., White, J., Barnard, E., Liu, J. and Brongersma, M.L. (2009) Design of Plasmonic Thin-Film Solar Cells with Broadband Absorption Enhancements. *Advanced Materials*, **21**, 3504-3509. <https://doi.org/10.1002/adma.200900331>
- [18] Lu, R.C. and Jang, Y.L. (2013) Coupling Device with Resonant Cavities Based on Periodic Dielectric Waveguides. *Optics and Photonics Journal*, **3**, 240-242. <https://doi.org/10.4236/opj.2013.32B056>
- [19] Atwater, H.A. and Polman, A. (2010) Plasmonics for Improved Photovoltaic Devices. *Nature Materials*, **9**, 205-213. <https://doi.org/10.1038/nmat2629>
- [20] Hryciw, A., Jun, Y.C. and Brongersma, M.L. (2010) Plasmonics: Electrifying Plasmonics on Silicon. *Nature Materials*, **9**, 3-4. <https://doi.org/10.1038/nmat2598>
- [21] Omelyanovich, M., Makarov, S., Milichko, V. and Simovski, C. (2016) Enhancement of Perovskite Solar Cells by Plasmonic Nanoparticles. *Materials Sciences and Applications*, **7**, 836-847. <https://doi.org/10.4236/msa.2016.712064>
- [22] Yu, N., Fan, J., Wang, Q.J., Pflügl, C., Diehl, L., Edamura, T., Capasso, F., *et al.* (2008) Small-Divergence Semiconductor Lasers by Plasmonic Collimation. *Nature Photonics*, **2**, 564-570. <https://doi.org/10.1038/nphoton.2008.152>
- [23] Oulton, R.F., Sorger, V.J., Zentgraf, T., Ma, R.M., Gladden, C., Dai, L. and Zhang, X. (2009) Plasmon Lasers at Deep Subwavelength Scale. *Nature*, **461**, 629-632. <https://doi.org/10.1038/nature08364>
- [24] Gao, N., Huang, K., Li, J., Li, S., Yang, X. and Kang, J. (2012) Surface-Plasmon-Enhanced Deep-UV Light Emitting Diodes Based on AlGa<sub>N</sub> Multi-Quantum Wells. *Scientific Reports*, **2**, Article No. 816. <https://doi.org/10.1038/srep00816>
- [25] Temnov, V.V. (2012) Ultrafast Acousto-Magneto-Plasmonics. *Nature Photonics*, **6**, 728-736. <https://doi.org/10.1038/nphoton.2012.220>
- [26] Ren, F.F., Ang, K.W., Ye, J., Yu, M., Lo, G.Q. and Kwong, D.L. (2011) Split Bull's Eye Shaped Aluminum Antenna for Plasmon-Enhanced Nanometer Scale Germanium Photodetector. *Nano Letters*, **11**, 1289-1293. <https://doi.org/10.1021/nl104338z>
- [27] Baffou, G. and Quidant, R. (2013) Thermo-Plasmonics: Using Metallic Nanostructures as Nano-Sources of Heat. *Laser & Photonics Reviews*, **7**, 171-187. <https://doi.org/10.1002/lpor.201200003>
- [28] Hirsch, L.R., Stafford, R.J., Bankson, J.A., Sershen, S.R., Rivera, B., Price, R.E., West, J.L., *et al.* (2003) Nanoshell-Mediated Near-Infrared Thermal Therapy of Tumors under Magnetic Resonance Guidance. *Proceedings of the National Academy of Sciences*, **100**, 13549-13554. <https://doi.org/10.1073/pnas.2232479100>
- [29] Li, Z., Wang, Y., He, J., Feng, D., Gu, E. and Li, W. (2016) An Ultraviolet Hybrid

- Plasmonic Waveguide for Nanolaser Applications. *Optics and Photonics Journal*, **6**, 19-23. <https://doi.org/10.4236/opj.2016.68B004>
- [30] Jing J. (2002) The Finite Element Method in Electromagnetics. 2nd Edition, Wiley, New York.
- [31] Yee, K. (1966) Numerical Solution of Initial Boundary Value Problems Involving Maxwell's Equations in Isotropic Media. *IEEE Transactions on Antennas and Propagation*, **14**, 302-307. <https://doi.org/10.1109/TAP.1966.1138693>
- [32] Van Roey, J., Van der Donk, J. and Lagasse, P.E. (1981) Beam-Propagation Method: Analysis and Assessment. *Journal of the Optical Society of America*, **71**, 803-810. <https://doi.org/10.1364/JOSA.71.000803>
- [33] Ney, M.M. (1985) Method of Moments as Applied to Electromagnetic Problems. *IEEE Transactions on Microwave Theory and Techniques*, **33**, 972-980. <https://doi.org/10.1109/TMTT.1985.1133158>
- [34] Le Ru, E. and Etchegoin, P. (2008) Principles of Surface-Enhanced Raman Spectroscopy: And Related Plasmonic Effects. Elsevier, Amsterdam. <https://doi.org/10.1016/B978-0-444-52779-0.00005-2>
- [35] Noual, A., Akjouj, A., Pennec, Y., Gillet, J.N. and Djafari-Rouhani, B. (2009) Modeling of Two-Dimensional Nanoscale Y-Bent Plasmonic Waveguides with Cavities for Demultiplexing of the Telecommunication Wavelengths. *New Journal of Physics*, **11**, Article ID: 103020. <https://doi.org/10.1088/1367-2630/11/10/103020>
- [36] Ordal, M.A., Bell, R.J., Alexander, R.W., Long, L.L. and Querry, M.R. (1985) Optical Properties of Fourteen Metals in the Infrared and Far Infrared: Al, Co, Cu, Au, Fe, Pb, Mo, Ni, Pd, Pt, Ag, Ti, V, and W. *Applied Optics*, **24**, 4493-4499. <https://doi.org/10.1364/AO.24.004493>
- [37] Keleshtery, M.H., Kaatuzian, H. and Mir, A. (2016) Analysis and Investigation of Slow Light Based on Plasmonic Induced Transparency in Metal-Dielectric-Metal Ring Resonator in a Waveguide System with Different Geometrical Designs. *Optics and Photonics Journal*, **6**, 177-184. <https://doi.org/10.4236/opj.2016.68B029>
- [38] Ghosh, S., Brahmachari, K. and Ray, M. (2012) Experimental Investigation of Surface Plasmon Resonance Using Tapered Cylindrical Light Guides with Metal-Dielectric Interface. *Journal of Sensor Technology*, **2**, 48-54. <https://doi.org/10.4236/jst.2012.21007>
- [39] Taheri, A.N. and Kaatuzian, H. (2013) Simulation and Design of a Submicron Ultrafast Plasmonic Switch Based on Nonlinear Doped Silicon MIM Waveguide. *Journal of Computer and Communications*, **1**, 23-26. <https://doi.org/10.4236/jcc.2013.17006>
- [40] Taflove, A. and Hagness, S.C. (2005) Computational Electrodynamics: The Finite-Difference Time-Domain Method. Artech House, Norwood. <https://doi.org/10.1002/0471654507.eme123>
- [41] Mashade, E., Bakry, M. and Abdel Aleem, M.N. (2009) Analysis of Ultra-Short Pulse Propagation in Nonlinear Optical Fiber. *Progress in Electromagnetics Research*, **12**, 219-241. <https://doi.org/10.2528/PIERB08121603>
- [42] Nady Abdul Aleem, M. (2017) Mode Splitting Based on the Coupling between Modes of Two Nanodisks Cavities and a Plasmonic Waveguide. *Progress in Electromagnetics Research*, **55**, 179-188. <https://doi.org/10.2528/PIERM17021407>
- [43] Xie, Y., Zakharian, A.R., Moloney, J.V. and Mansuripur, M. (2004) Transmission of Light through Slit Apertures in Metallic Films. *Optics Express*, **12**, 6106-6121. <https://doi.org/10.1364/OPEX.12.006106>

- [44] Schouten, H.F., Visser, T.D., Lenstra, D. and Blok, H. (2003) Light Transmission through a Subwavelength Slit: Waveguiding and Optical Vortices. *Physical Review E*, **67**, Article ID: 036608. <https://doi.org/10.1103/PhysRevE.67.036608>
- [45] Mansuripur, M., Xie, Y., Zakharian, A.R. and Moloney, J.V. (2005) Transmission of Light through Slit Apertures in Metallic Films. *IEEE Transactions on Magnetics*, **41**, 1012-1015. <https://doi.org/10.1109/TMAG.2004.842048>